

# ResAdapter: Domain Consistent Resolution Adapter for Diffusion Models

Jiaxiang Cheng Pan Xie<sup>†</sup> Xin Xia Jiashi Li Jie Wu  
Yuxi Ren Huixia Li Xuefeng Xiao Min Zheng Lean Fu  
ByteDance Inc

{chengjiaxiang, xiepan.01, xiabin.97, lijiaoshi, wujie.10}@bytedance.com  
{renyuxi.20190622, lihuixia, xiaoxuefeng.ailab, zhengmin.666, fulean}@bytedance.com

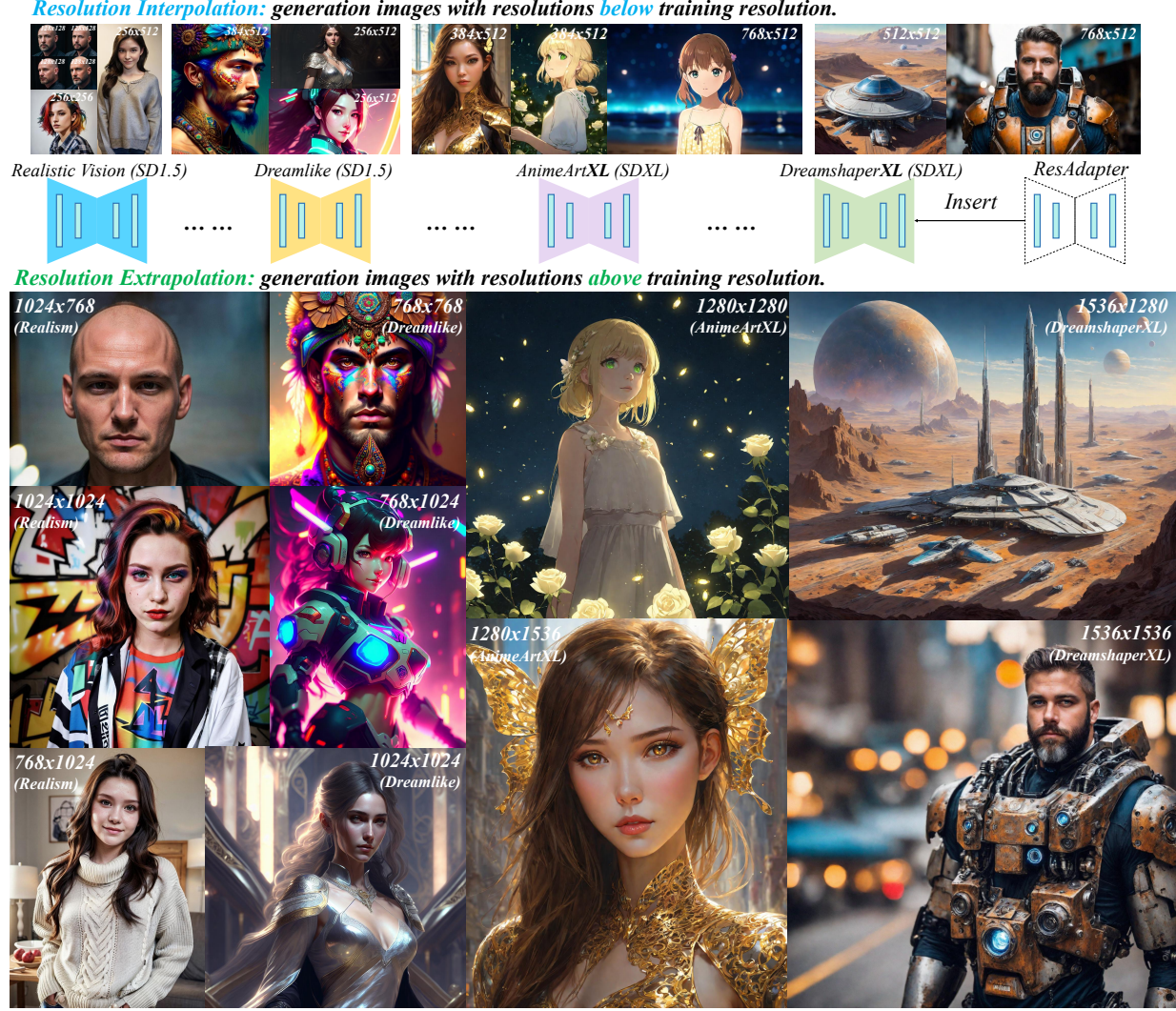


Figure 1. We propose **ResAdapter**, a plug-and-play adapter for enabling the resolution extrapolation and interpolation of diffusion models of arbitrary style domain. **Resolution Extrapolation**: generate images with resolutions above their trained resolution (e.g.,  $1536 \times 1536$ ). **Resolution Interpolation**: generate images with resolutions below their trained resolution (e.g.,  $128 \times 128$ ). Once learning resolution priors, ResAdapter can be integrated into diffusion models to generate images with unrestricted resolutions and aspect ratio while preserving their original style domain. More results are in Appendix 8.

## Abstract

Recent advancement in text-to-image models (e.g., Stable Diffusion) and corresponding personalized technologies (e.g., DreamBooth and LoRA) enables individuals to gen-

erate high-quality and imaginative images. However, they often suffer from limitations when generating images with resolutions outside of their trained domain. To overcome this limitation, we present the **Resolution Adapter (ResAdapter)**, a domain-consistent adapter designed for diffusion models to generate images with unrestricted resolutions and aspect

<sup>†</sup>Corresponding author

ratios. Unlike other multi-resolution generation methods that process images of static resolution with complex post-process operations, ResAdapter directly generates images with the dynamical resolution. Especially, after learning a deep understanding of pure resolution priors, ResAdapter trained on the general dataset, generates resolution-free images with personalized diffusion models while preserving their original style domain. Comprehensive experiments demonstrate that ResAdapter with only 0.5M can process images with flexible resolutions for arbitrary diffusion models. More extended experiments demonstrate that ResAdapter is compatible with other modules (e.g., ControlNet, IP-Adapter and LCM-LoRA) for image generation across a broad range of resolutions, and can be integrated into other multi-resolution model (e.g., ElasticDiffusion) for efficiently generating higher-resolution images. Project link <https://resadapter.github.io/>.

## 1. Introduction

Diffusion models [13, 36, 38] have experienced a remarkable surge in their capabilities and applications [22, 25, 29]. Among them, Stable Diffusion (SD) [30] and SDXL [27] are pre-trained models on the large-scale dataset LAION-5B [33], having emerged as powerful generative models. Additionally, the open-source community has been enriched by numerous personalized diffusion models from CivitAI [4], trained with DreamBooth [32] or Low-rank Adaptation (LoRA) [15]. They are capable of generating imaginative high-quality images at the training resolution (e.g.,  $512 \times 512$  for SD-based models and  $1024 \times 1024$  for SDXL-based models) using the given prompts. However, they often suffer from limitations when generating images with resolutions outside of their trained domain. As shown in Fig. 2, the SD-based model and the personalized diffusion model generate lower-resolution images (e.g.,  $256 \times 256$ ) with the poor fidelity and higher-resolution images (e.g.,  $1024 \times 1024$ ) with the poor framing and composition. As a result, we can name this phenomena as the *resolution domain inconsistent*.

Existing work is categorized into two main research directions to address this limitation. The first research line is post-processing [1, 9, 16], represented by MultiDiffusion [1] and ElasticDiffusion [9], where images with resolutions in their trained domain are repeatedly processed and then stitched together to generate images with flexible resolutions through overlap. However, this approach often takes longer inference time with complex post-process operations. The second research line is straightforward. Fine-tuning on a broader range of resolutions to empower diffusion models to generate resolution-free images with LoRA [15]. However, most personalized models in CivitAI [4] do not provide details about their training datasets. Fine-tuning on the general dataset like LAION-5B [33] inevitably influences their original style domain, which is shown in Fig. 2. We name this phenomena

Table 1. **Comparison of ResAdapter and other methods.** **Domain consistent:** resolution and style domain of generation image maintain consistent for arbitrary diffusion models. **Module compatible:** compatible with other modules except diffusion models. **Training inexpensive:** low-cost training. **Inference efficient:** process images without repeated denoising steps and complex post-process operations.

Method	Domain Consistent	Module Compatible	Training Inexpensive	Inference Efficient
SDXL [27]	×	×	×	✓
LoRA [15]	×	✓	✓	✓
DiffFit [41]	×	×	✓	✓
Mixture-of-Diffuser [16]	×	×	✓	×
MultiDiffusion [1]	×	×	✓	×
Any-Size-Diffusion [46]	×	×	×	×
ElasticDiffusion [9]	×	×	✓	×
ResAdapter	✓	✓	✓	✓

as the *style domain inconsistent*.

**Can we train a plug-and-play resolution adapter to generate images with unrestricted resolutions and aspect ratio for arbitrary diffusion models?** To answer this question, we decompose it into three dimensions: (1) **resolution interpolation:** generate images with resolutions below the trained resolution of diffusion models. (2) **resolution extrapolation:** process images with resolutions above the trained resolution of diffusion models. (3) **style domain consistency:** generate images without transforming the original style domain of the diffusion model.

We analyze the structure of UNet’s blocks [31], finding that the attention and MLP are both content-sensitive layers, which are sensitive to the style information of images compared to resolution. But the convolution layers with fixed receptive file are resolution-sensitive, meaning they are easily influenced by the resolution of generation images. Leveraging these finds, we present the resolution convolution LoRA (**ResCLORA**) for dynamically matching the receptive filed of convolution and the feature map size of images with flexible resolutions. However, we find that as the resolution increases, the gap about the quality of generation images increases between LoRA [15] and full fine-tuning, which is as shown in Fig. 4. We attribute it into the inability of normalization in UNet’s blocks to adapt the statistical distribution of images in resolution extrapolation. According to this, we present the resolution extrapolation normalization (**ResENorm**) for reducing the gap between LoRA and full fine-tuning in resolution extrapolation. To enable the style domain consistency, we optimize the position of ResCLORA and ResENorm insertions on UNet’s blocks to guide them to learn resolution priors ignoring the style information from the general datasets.

By integrating these two optimized methods, we can obtain a plug-and-play domain-consistent resolution adapter (**ResAdapter**), which expands the range of resolution do-



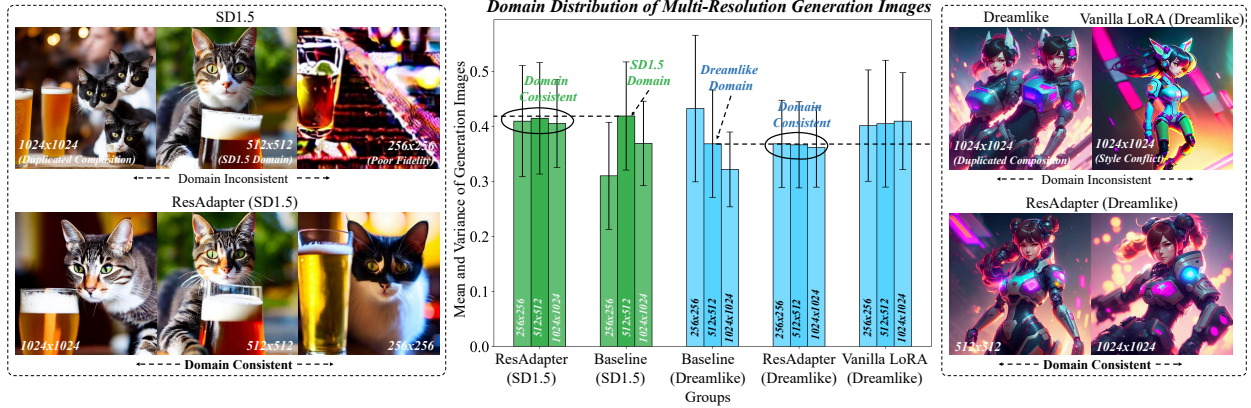


Figure 2. **Motivation.** We explore the domain of images generated by SD1.5 (Left) [30] and Dreamlike (Right) at resolutions of  $256 \times 256$ ,  $512 \times 512$  and  $1024 \times 1024$ . Dreamlike is the personalized diffusion model based on SD1.5. ResAdapter and vanilla LoRA are both trained on LAION-5B [33], their structures are shown in Fig. 3. **Baselines** transform domains at resolutions of  $256 \times 256$  and  $1024 \times 1024$ . **ResAdapter** keep domain consistent at different resolutions. **Vanilla LoRA** [15] injects style priors from LAION-5B and influences the Dreamlike domain, resulting to low-quality images with the style conflict.

main from the diffusion models without transforming their original style domains. Our main experiments demonstrate that after learning resolution priors, ResAdapter with only 0.5M can expand the generation resolution of arbitrary diffusion models based SD from  $128 \times 128$  to  $1024 \times 1024$  and scale the SDXL-based diffusion models from  $256 \times 256$  to  $1536 \times 1536$ , as shown in Fig. 1. Our extensive experiments demonstrate that ResAdapter is compatible with other modules (e.g., ControlNet [44] for conditional generation, IP-Adapter for image generation based on the image prompt and LCM-LoRA [23] for accelerating generation), and even can be integrated into other multi-resolution models (e.g., ElasticDiffusion [9]) for efficiently generating  $2048 \times 2048$  high-resolution images. Detailed comparison with other related work is summarized in Table 1.

Our contributions can be summarized as follows:

- We present a plug-and-play domain-consistent ResAdapter for generating images of resolution interpolation and extrapolation with diffusion models.
- ResAdapter enables diffusion models of arbitrary style domain to generate images of unrestricted resolution and aspect ratio without transforming their style domain.
- ResAdapter is lightweight and without complex post-process operations. We can train it for only 0.5M with low-cost consumption and efficiently inference resolution-free images.
- ResAdapter is compatible with other modules to generate images with flexible resolution, such as ControlNet [44], IP-Adapter [43] and LCM-LoRA [23], even can optimize generation efficiency of other multi-resolution models such as ElasticDiffusion [9].

## 2. Related Work

### 2.1. Text-to-Image Generation

The rapid development of Artificial Intelligence Generative Component (AIGC) has attracted growing interest in Text-to-Image Generation (TTI). Early GAN-based methods [8, 26, 28] employ small-scale data for training but encounter challenges in adapting to large-scale data due to the instability of the adversarial training process. Autoregressive-based methods [6, 19, 39] learn the latent distribution of discrete latent spaces but take more inference costs. Recently, diffusion models [5, 13, 17, 38] has emerged as the state-of-the-art (SOTA) model in TTI field. The diffusion models represented by Stable Diffusion [30] and SDXL [27] contribute to high-resolution image generation. With the advent of personalized techniques [15, 32], they are capable of generating imaginative images. However, they still encounter limitations in resolution extrapolation and interpolation.

### 2.2. Multi-Resolution Image Generation

Existing work of multi-resolution image generation mainly utilizes post-processing to generate images beyond the training resolution. Mixture-of-Diffusers [16] and MultiDiffusion [1] utilize pre-trained Stable Diffusion [30] to generate  $512 \times 512$  images multiple times, and overlap to generate high-resolution landscape images. But this also lead to duplicated objects. Any-Size-Diffusion [46] fine-tunes on multi-aspect ratio images, and generates high-resolution images through implicit overlap. ElasticDiffusion [9] optimizes the post-processing process and can generate lower resolution images. Compared to these work, our ResAdapter does not require post-processing that take more inference time and can be integrated into any personalized model. ResAdapter can even be combined with these work to optimize inference time of generating higher resolution images.

### 2.3. Parameters-Efficient Fine-Tuning

With the emergence of large-scale datasets [33], the parameter count of diffusion models has reached the billion level. Full-parameter fine-tuning [27] takes high training costs in specific downstream tasks, while also leading to catastrophic forgetting [7, 24, 35]. There are two kind approaches of PEFT applied to diffusion models: One is Adapter [2, 14, 15]. Inserting extra modules on the base model. LoRA [15] inserts two low-rank matrices on the query and value of the attention to learn the knowledge of the downstream task. Another is Partial Parameter Tuning [20, 41, 42]. DiffFit [41] unfreezes partial weights and biases of the base model to learn the new domain. However, they can not integrated into any personalized model. They both transform the style domain of the personalized model, leading to the style conflict, shown in Fig.2 and Fig.16.

## 3. Background

In this section, we provide a brief review of the definition and principles of Denoise Diffusion Model [13] (Sec.3.1) and Stable Diffusion Model [30] (Sec.3.2).

### 3.1. Denoise Diffusion Model

The generation process of the diffusion model involves both forward diffusion and reverse denoise processes. Given a data sample  $x_0 \sim q_{data}(x)$ , diffusion model gradually injects small gaussian noise into data and generates samples through reverse denoise. Specifically, the *forward diffusion process* of the diffusion model is controlled by a Markov chain as  $q(x_t|x_{t-1}) = \mathcal{N}(x_t; \sqrt{1-\beta_t}x_{t-1}, \beta_t I)$ , where  $\beta_t$  is a variance schedule between 0 and 1. The data distribution  $q_{data}(x)$  can be transformed into a marginal distribution  $q(x_t|x_0)$  by employing reparameterization tricks. Using notation  $\alpha_t := 1 - \beta_t$  and  $\bar{\alpha}_t := \prod_{s=1}^t \alpha_s$ , we have  $q(x_t|x_0) = \mathcal{N}(x_t; \sqrt{\bar{\alpha}_t}x_0, (1 - \bar{\alpha}_t)I)$ .

Considering the *reverse process*, the diffusion model learns to progressively reduce small gaussian noise as:  $p_\theta(x_{t-1}|x_t) = \mathcal{N}(x_{t-1}; \mu_\theta(x_t, t), \sigma_t^2 I)$ , where  $\mu_\theta(x_t, t) = \frac{1}{\sqrt{\alpha_t}}(x_t - \frac{\beta_t}{\sqrt{1-\bar{\alpha}_t}}\epsilon_\theta(x_t, t))$ . The corresponding objective function is the variational lower bound of the negative log-likelihood. We get the equation as  $\mathcal{L}(\theta) = \sum_t \mathcal{D}_{KL}(q(x_{t-1}|x_t, x_0)|p_\theta(x_{t-1}|x_t)) - p_\theta(x_0|x_1)$ , where  $\mathcal{D}_{KL}$  denotes KL divergence between distribution  $p$  and  $q$ . Furthermore, through the parameterization  $\mu_\theta(x_t, t)$ , the loss function can be simplified as:

$$L_{\text{simple}} = \mathbb{E}_{x_0, \epsilon, t} [||\epsilon - \epsilon_\theta(\sqrt{\bar{\alpha}_t}x_0 + \sqrt{1-\bar{\alpha}_t}\epsilon, t)||^2] \quad (1)$$

The training objective in this formulation is minimizing the squared error between the gaussian noise and the estimated noise of the noise-added samples.

### 3.2. Stable Diffusion Model

To reduce the training cost of the diffusion model and generate high-resolution images, Stable Diffusion (SD) [30] encodes the image using variational autoencoder [39]. SD performs forward diffusion and reverse denoise in the latent space. Specifically, given a data  $x_0 \sim q_{data}(x)$ , the encoder  $\mathcal{E}$  encodes the image into latent representation  $z_0 = \mathcal{E}(x_0)$ . For the latent representation  $\tilde{z}$  generated by the diffusion model in the latent space, the decoder  $\mathcal{D}$  can reconstruct it into an image  $\tilde{x}$ . The encoder usually downsamples the image by a factor  $f = 8$  in SD. According to Sec.3.1, we have a simple loss function for SD:

$$L_{\text{simple}} = \mathbb{E}_{z_0, \epsilon, t} [||\epsilon - \epsilon_\theta(\sqrt{\bar{\alpha}_t}z_0 + \sqrt{1-\bar{\alpha}_t}\epsilon, t)||^2] \quad (2)$$

The architecture of UNet's blocks is shown in Fig.3. Each block catains three components: resnet layer  $\mathcal{W}_r$  [10], attention layer  $\mathcal{W}_a$  [40], downsampler  $\mathcal{W}_d$  or upsampler  $\mathcal{W}_u$ .

## 4. Method

In this section, we delve into our proposed plug-and-play domain-consistent ResAdapter, which enables diffusion models of arbitrary style domain to generate images with unrestricted resolutions and aspect ratio. In Sec.4.1, we introduce ResCLoRA, which enables diffusion models to generate images with resolution interpolation. In Sec.4.2, we introduce ResENorm, which compensates for the lack of capability about ResCLoRA in resolution extrapolation. In Sec.4.3, we present a simple multi-resolution training strategy, which can effectively make diffusion models generate images with flexible resolutions through only one ResAdapter.

### 4.1. Resolution Interpolation

Vanilla LoRA [15] enables the base model (e.g., SD [30] and SDXL [27]) to generate high-quality style images. As shown in Fig.3(b), vanilla LoRA is inserted into the query, value, key and output layers of the attention block to learn the style domain distribution of images. It is defined as  $\mathcal{W}'_a = \mathcal{W}_a + \Delta\mathcal{W} = \mathcal{W}_a + AB^T$ , where  $A \in \mathbb{R}^{m \times r}$ ,  $B \in \mathbb{R}^{n \times r}$  are two rank-decomposition matrices,  $r$  represents the rank of matrices. However, the vanilla LoRA trained on the general datasets can not be integrated into other personalized diffusion models, which influences their original style domain. As shown in Fig.2, vanilla LoRA trained on LAION-5B [33] transforms the domain of Dreamlike to the domain of SD1.5 and generates bad quality images with style conflicts.

ResCLoRA can be integrated into any personalized model to enable resolution interpolation for high-quality images without transforming the style domain. As described in Sec.1, the reason that leads to the poor fidelity of images with resolution interpolation is that the convolution with



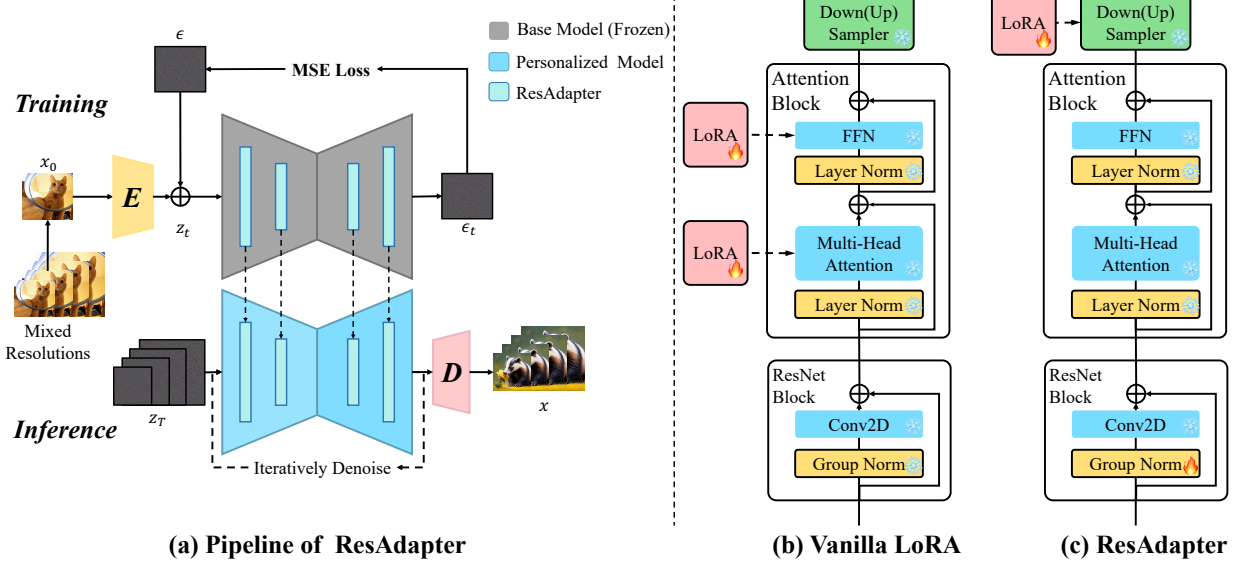


Figure 3. **Overview of ResAdapter.** **Left:** Pipeline of ResAdapter. ResAdapter based on the frozen model (e.g., SD [30] or SDXL [27]) learns resolution priors from mixed-resolution general datasets, and can be integrated into arbitrary personalized models to generate multi-resolution images. **Right:** Architecture comparison between ResAdapter and the vanilla LoRA [15]. Compared to vanilla LoRA, ResAdapter is only inserted to downsampler and upsampler, and it unfreezes the group normalization of resnet blocks.

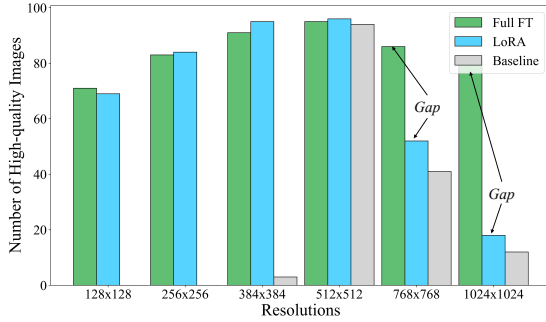


Figure 4. High-quality images represent without poor fidelity or composition. We train SD1.5 with LoRA [15] and full fine-tuning on LAION-5B [33] ranging from  $128 \times 128$  to  $1024 \times 1024$  resolution. We sample 100 images using for each resolution, respectively. We find that as the resolution increases, the gap between LoRA and full fine-tuning becomes larger.

the fixed receptive field is sensitive to the resolution of images. According to this, ResCLORA is inserted into the convolution layers of UNet’s blocks to learn resolution priors. To prevent as much as possible ResCLORA from capturing the style domain of the general datasets, it is only inserted into the convolution layers in downsampler and upsampler. We define ResCLORA as  $\mathcal{W}'_d = \mathcal{W}_d + AB^T$  and  $\mathcal{W}'_u = \mathcal{W}_u + AB^T$ , which is shown in Fig.3(c). Compared to the style information, the resolution information is low-level knowledge. Thus, ResCLORA with only 0.4M can provide the rich resolution prior for the personalized model, adaptively adjusting the receptive field of the convolution in UNet’s blocks to match the feature map size of generation images while preserving their style domain.

## 4.2. Resolution Extrapolation

Our initial experiment finds that there is a large gap as the resolution increases between LoRA and full fine-tuning, as shown in Fig.4. This means that only ResCLORA does not enable the resolution extrapolation ability of the personalized model. For example, ResCLORA integrated into the diffusion model still generates higher-resolution images with poor framing and composition. Inspired by [3], we find that the failure of the resolution extrapolation is limited by the ability of normalization layers. Existing normalization layers can not adapt to the statistical distribution of feature maps of higher-resolution images.

However, we find that if all the normalization layers in UNet’s blocks are trained on the general dataset, the trained weights are incompatible with other personalized diffusion models, which leads to low-quality images with poor style color, as shown in Appendix.9. However, we find that all normalization layers of UNet’s blocks trained on LAION-5B [34] are not compatible with the other parameters of the personalized model, which still leads to low-quality images with poor style color, as shown in Fig.16. In order to keep the original style domain of generation images, we need to maintain partial normalization layers of the personalized model. As shown in Fig.3(c), we only open group normalization of resnet layer, which is named as ResENorm. It not only reduce the gap about the resolution prior between ResCLORA and full fine-tuning, but also helps retain the style domain of the personalized model. Additionally, we only train ResENorm in resolution extrapolation for better adapting to the statistical distribution of the feature map

of higher-resolution images. After that, ResENorm with ResCLoRA can improve the poor framing and composition of generation images. Especially, ResENorm only occupies 0.1M parameters but make effects for reducing the gap in resolution extrapolation.

### 4.3. Multi-Resolution Training

To enable multi-resolution image generation for single ResAdapter, we propose a simple mixed-resolution training strategy, as shown in Fig.3(a). For SD [30], we train on the mixed datasets with common resolutions from  $128 \times 128$  to  $1024 \times 1024$  with unrestricted aspect ratio. For SDXL [27], we train on the mixed datasets with common resolutions from  $256 \times 256$  to  $1536 \times 1536$  with unrestricted aspect ratio. The multi-resolution training strategy allows ResAdapter to learn multi-resolution knowledge simultaneously and prevents catastrophic forgetting [7, 24, 35].

Our experiments find that lower and higher resolution images (e.g.,  $128 \times 128$  and  $1024 \times 1024$  for SD) are more difficult to train. To alleviate this phenomenon, we use a simple probability function to sample images at the different training resolution. It is defined as  $p(x) = |x-r|^2 / \sum_i^N |x_i-r|^2$ , where  $r$  represents the standard resolution (e.g.,  $512 \times 512$  for SD). This can improve the probability of selecting lower or higher resolution images resolution during the multi-resolution training process. More training details are provided in Sec.5.1.

## 5. Experiment

In this section, we present the experimental setup and experimental results of ResAdapter. In Sec.5.1, we describe the experimental setup in detail, including training details, evaluation metrics, and the selection of personalized models. In Sec.5.2, we show the main experimental results. We compare ResAdapter with other multi-resolution image generation models as well as the original personalized model. In Sec.5.3, we show the extended experimental results. That is the application of ResAdapter in combination with other modules. In Sec.5.4, we perform ablation experiments about modules and alpha of ResAdapter.

### 5.1. Experiment Setup

**Training Details.** We train ResAdapter using the large-scale dataset LAION-5B [33]. Considering most structures of personalized models in the open-source community, we choose SD1.5 [30] and SDXL [27] as the base models. For SD1.5, we train on images with  $128 \times 128$ ,  $256 \times 256$ ,  $384 \times 384$ ,  $768 \times 768$  and  $1024 \times 1024$  resolutions. For SDXL, we expanded the training resolution range to  $256 \times 256$ ,  $384 \times 384$ ,  $512 \times 512$ ,  $768 \times 768$ ,  $1280 \times 1280$ ,  $1408 \times 1408$ , and  $1536 \times 1536$ . Meanwhile, the training dataset contains images with different ratios such as 4:3, 3:4, 3:2, 2:3, 16:9 and 9:16, etc. For SD1.5 and SDXL, we both use a batch size

Table 2. **Personalized models** used for evaluation. We selected representative personalize models from CivitAI [4] for evaluation in domain-consistent experiments, which cover domains ranging from 2D anime to real photographs.

Model Name	Domain	Model Type	Training Type
Dreamshaper	Stylistic	SD1.5 [30]	DreamBooth
Dreamlike	Illustration		DreamBooth
Cuteyukimix	Cute		DreamBooth
RealisticVision	Realist		DreamBooth
SamaritanXL	3D Cartoon	SDXL1.0 [27]	LoRA
AnimeArtXL	Anime		LoRA
JuggernautXL	Realistic		DreamBooth
DreamshaperXL	Stylistic		DreamBooth

of 32 and a learning rate of  $1e-4$  for training. We use the AdamW optimizer [18] with  $\beta_1 = 0.95$ ,  $\beta_2 = 0.99$ . The total number of training steps is 20,000. Since ResAdapter is only 0.5M of trainable parameters, we train it for less than an hours on 8xA100 GPUs.

**Evaluation Metrics.** For experiments comparing ResAdapter with the personalized model, we hire 5 humans to participating in the qualitative evaluation. For experiments comparing ResAdapter and the other multi-resolution image generation models, we refer to ElasticDiffusion [9] and use Fréchet Inception Distance (FID) [12] and CLIP Score [11] as evaluation metrics. They evaluate the quality of the generated images and the degree of alignment between the generated images and prompts. For other multi-resolution generation models, we chose MultiDiffusion (MD) [1] and ElasticDiffusion (ED) [9] as baselines.

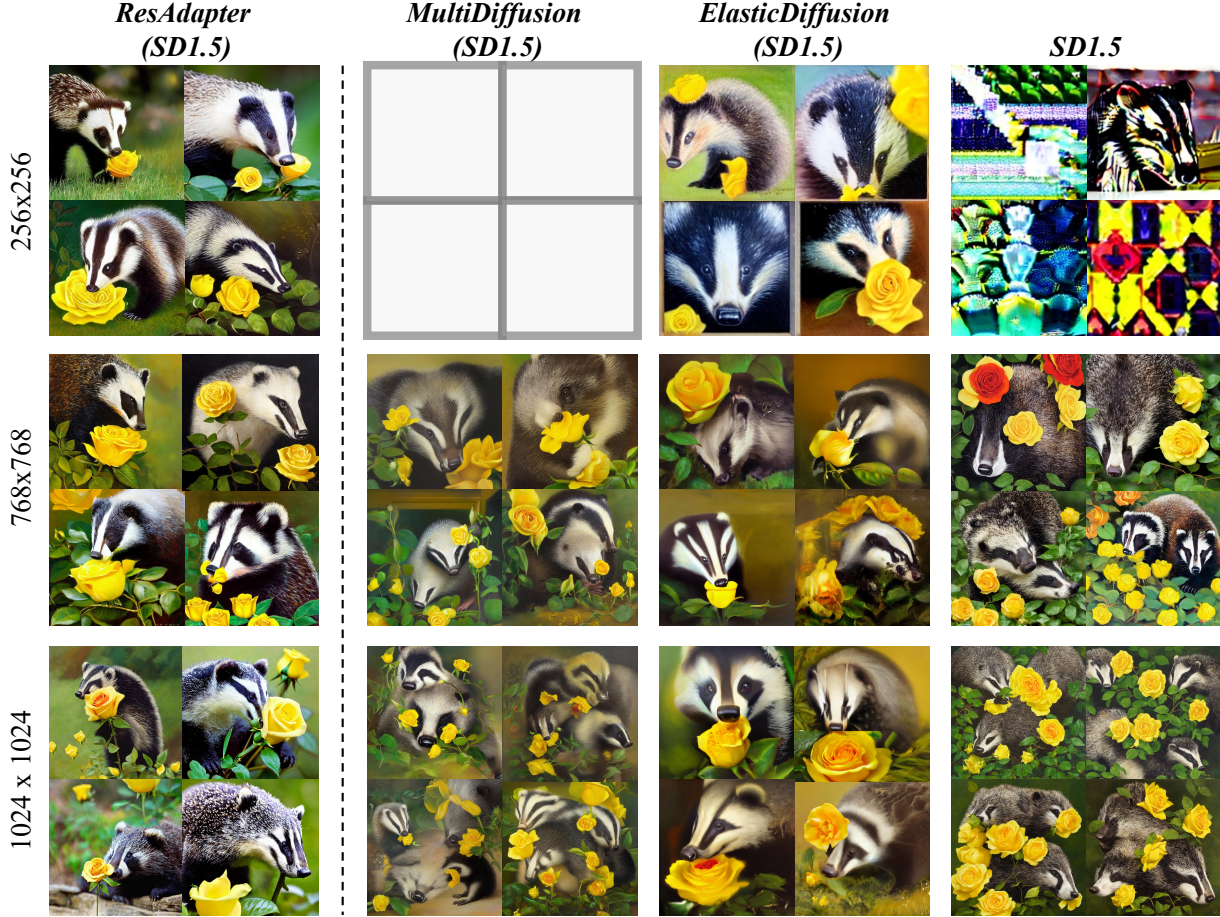
**Personalized Models.** In order to demonstrate the effectiveness of our ResAdapter, we choose multiple personalized models from Civitai [4], which cover a wide domains range from 2D animation to realistic photography. More detailed information is provided in Table 2.

### 5.2. Main Results

**Comparison with Multi-Resolution Generation Models.** For *qualitative results*, see Fig.5. We compare the image performance of MultiDiffusion (MD) [1] and ElasticDiffusion (ED) [9] with our ResAdapter at the resolutions of  $256 \times 256$ ,  $768 \times 768$  and  $1024 \times 1024$ .

The qualitative results demonstrate that ResAdapter generates multi-resolution images of better quality compared with MD and ED. MD generates higher-resolution images with the poor framing and composition, and can not generate lower-resolution images than the training resolution. ED generates the images with more inference time. ResAdapter significantly improves the quality of multi-resolution images. For *quantitative results*, see Table 3. The results show that ResAdapter outperforms MD and ED in terms of FID and CLIP Score. About the latency time, ResAdapter without post-processing is, on average, 9 times faster compared





Prompt: A young badger delicately sniffing a yellow rose.

Figure 5. **Qualitative results** of ResAdapter and other multi-resolution generation models. Blank images indicate that the model can not generate images with that resolution.

Table 3. **Quantitative results** on LAION-COCO [34] at resolutions of  $256 \times 256$  and  $1024 \times 1024$ . #Calls represents the number of inference iterations at each noise reduction step. We measure the latency time of one step on an A100-80G.

Size	Method	FID(↓)	CLIP(↑)	#Call	Latency Time/(s)
256x256	SD <sub>1.4</sub> [30]	54.06	21.43	2	0.025
	SDXL [27]	175.87	14.60	2	0.038
	ElasticDiffusion <sub>1.4</sub> [9]	23.77	26.30	2	0.288
	<b>ResAdapter<sub>1.4</sub></b>	<b>23.01</b>	<b>26.98</b>	2	<b>0.025</b>
512x512	SD <sub>1.4</sub> [30]	20.50	27.33	2	0.0714
	<b>ResAdapter<sub>1.4</sub></b>	20.53	27.32	2	0.0714
1024x1024	SD [30]	47.01	25.70	2	0.1322
	SDXL [27]	25.58	<b>28.06</b>	2	0.1322
	MultiDiffusion <sub>1.4</sub> [1]	37.70	26.96	162	2.50
	ElasticDiffusion [9]	27.76	26.07	33	1.16
	<b>ResAdapter<sub>1.4</sub></b>	<b>26.89</b>	27.26	2	<b>0.1322</b>

to ED. We measure the latency time of one step on single A100-80G.

**Comparison with Personalized Models.** For *qualitative results*, see Fig. 6. To ensure the fairness of the experiments, we generate multi-resolution images using prompts

Table 4. **Human side-by-side evaluations** about text-to-image generation of ResAdapter and the personalized model.

Model Name	Size	Ratio	Good(G)	Same(S)	Bad(B)	(G+S)/(B+S)
RealisticVision	256	4:3	3321	1090	589	2.63
		3:4	3302	1102	596	2.59
	1024	16:9	2877	1563	560	2.09
		9:16	2978	1531	491	2.23
SamaritanXL	384	4:3	4613	338	49	12.79
		3:4	4684	249	67	15.61
	1536	16:9	2863	1566	571	2.07
		9:16	3009	1071	920	2.05

from Civitai [4]. These images are generated by ResAdapter and the personalized model. Lower-resolution images (e.g.,  $256 \times 256$ ,  $384 \times 384$ ) generated by the personalized model are significantly lower in terms of the images of the fidelity, while higher-resolution images (e.g.,  $1536 \times 1536$ ) suffer from the poor framing and composition. After integrating our ResAdapter into the personalized model, the fidelity and the composition of generation images are significantly im-



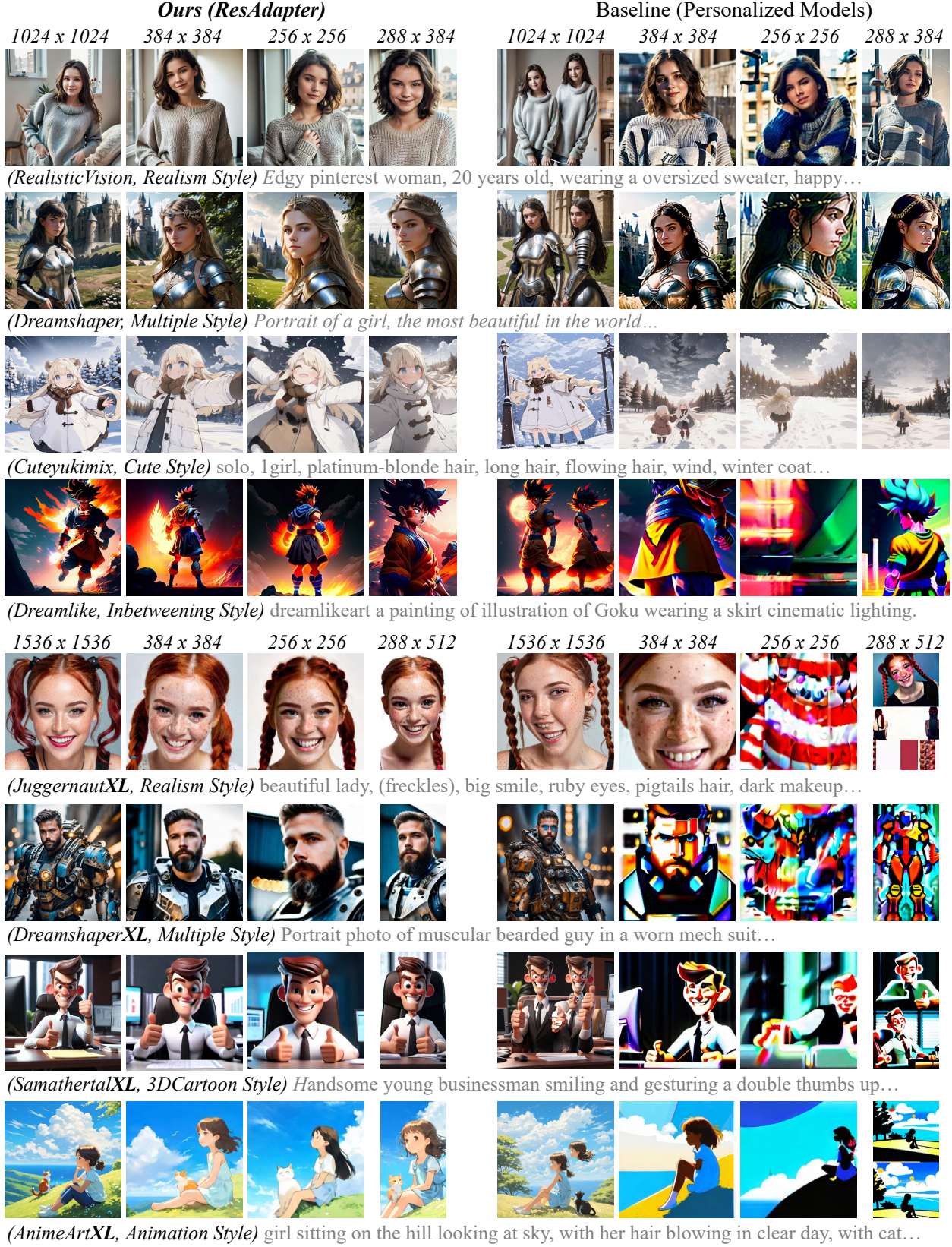


Figure 6. **Qualitative results.** We compare the multi-resolution images generated by ResAdapter and the personalized models. **Left:** Generation images from ResAdapter integrated into the personalized model. **Right:** Generation images from the original personalized model. Some prompts are edited for clarity. **XL** represent the personalize model based on SDXL [27]. More information about the personalized diffusion models is in Table 2 .



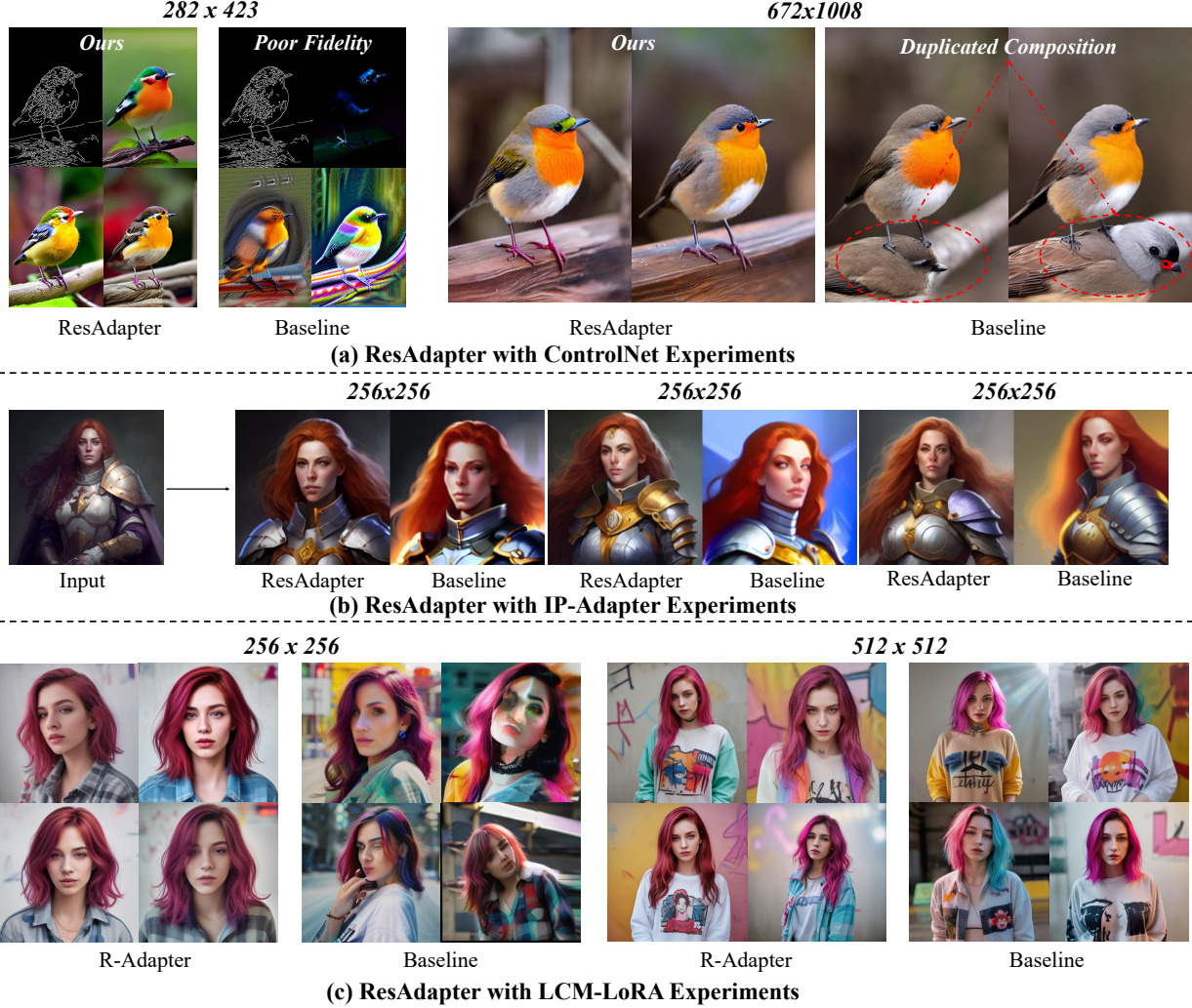


Figure 7. **Qualitative results** of extended experiments with ResAdapter. **Top:** Image-to-image tasks with ControlNet [44]. The condition is canny images at different resolution. **Middle:** Image variation tasks with IP-Adapter [43]. We resize the input image from 1024x1024 to 256x256. **Bottom:** Accelerating text-to-image tasks with LCM-LoRA [23]. We generate images in 4 steps. More results in Appendix 8.

proved. ResAdapter enables the resolution extrapolation and interpolation of the personalized model. For *quantitative results*, see Table 2. We evaluate the image quality by four criteria, which are the fidelity, the composition, the prompt alignment and the style domain consistency. The quantitative results demonstrate that ResAdapter significantly outperforms the personalized model, particularly in lower-resolution images.

### 5.3. Extended Results

**ResAdapter with ControlNet.** ControlNet [44] is a conditional control module that can utilize conditional images to control the generation of layout-specific images for SD [30]. As shown in Fig. 7, ControlNet generates low-quality images with poor fidelity and composition in the image-to-image task. While ResAdapter is compatible with ControlNet to

enable the resolution extrapolation and interpolation, improving the quality of images.

**ResAdapter with IP-Adapter.** IP-Adapter [43] is a adapter for image generation with the image prompt. As shown in Fig. 7, ResAdapter with IP-Adapter can generate high-quality images in the image variation task.

**ResAdapter with LCM-LoRA.** LCM-LoRA [23] is a module for accelerated image generation capable of generating high-quality images in 4 steps. As shown in Fig. 7, ResAdapter is integrated into the personalized model and compatible with LCM-LoRA. ResAdapter improves the fidelity of lower-resolution image while not degrades the quality of  $512 \times 512$  images.

**ResAdapter with ElasticDiffusion.** ResAdapter combined with other multi-resolution image generation models of post-processing can optimize the inference time. Specif-

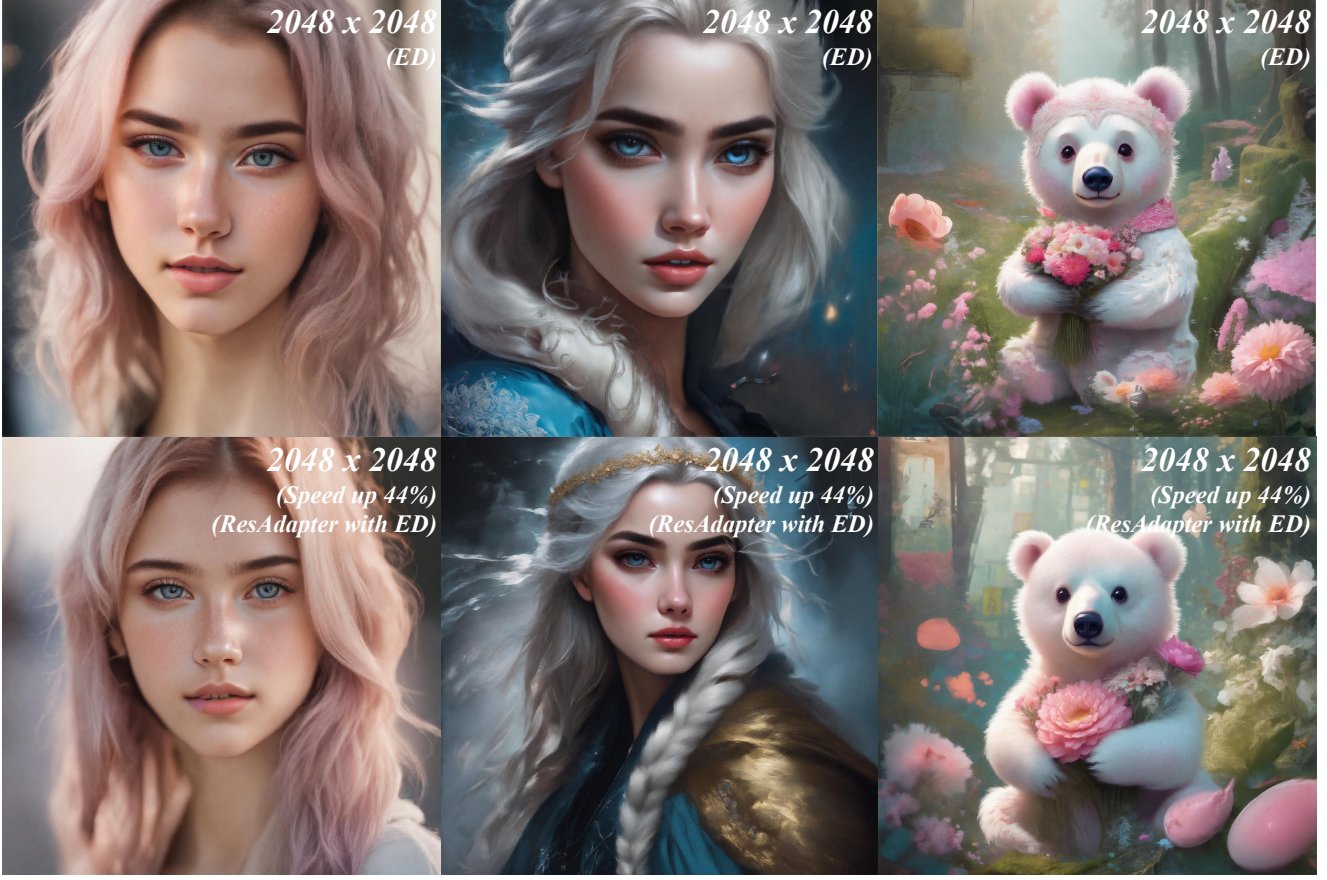


Figure 8. **Qualitative results** about ResAdapter with ElasticDiffusion (ED) [9]. **Top:** DreamshaperXL (ED) generates  $2048 \times 2048$  images by the post-process technology and uses  $1024 \times 1024$  as the standard resolution. **Bottom:** DreamshaperXL (ResAdapter with ED), generates  $2048 \times 2048$  images by the post-process technology and uses  $768 \times 768$  as the standard resolution, which efficiently optimizes the inference time.

ically, ElasticDiffusion (ED) [9] requires to inference the  $1024 \times 1024$  images multiple times, and overlaps them to get the  $2048 \times 2048$  images with the post-process technology, which takes much inference time. In order to optimize the inference time, we combine ResAdapter with ED to inference the  $768 \times 768$  images same times and overlap them to get  $2048 \times 2048$  images. As shown in Fig.8, ResAdapter with ED can generate  $2048 \times 2048$  images while no degradation of image quality compared with ED. Our ResAdapter can speed up the inference time by 44%. This demonstrates that ResAdapter can be flexibly applied to multiple scenarios.

#### 5.4. Ablation Study

For the modules of ResAdapter, we ablate on ResCLoRA and ResENorm, as shown in Fig.9(a). Without ResCLoRA or ResENorm, the duplicated composition of generation images still exists, which demonstrate the importance of their simultaneous presence. Compared with baseline, ResAdapter can generate images without transforming the original style domain. For alpha  $\alpha_r$  for ResAdapter, we make the ablation

study on  $\alpha_r$ , as shown in Fig.9(b). We find the quality of generation images increases as  $\alpha_r$  from 0 to 1.

## 6. Conclusion

In this paper, we present a plug-and-play domain-consistent ResAdapter for diffusion models of arbitrary style domain, which enables the resolution extrapolation and interpolation of generation images. Our experiments demonstrate that after a low-cost training, ResAdapter with only 0.5M can be integrated into diffusion models to generate high-quality images of unrestricted resolutions and aspect without transforming the original style domain. Our extended experiments also demonstrate ResAdapter is compatible with other modules (e.g., ControlNet [44], IP-Adapter [43] and LCM-LoRA [23]). In addition, ResAdapter can be combined with other multi-resolution image generation models (e.g., ElasticDiffusion [9]) to optimize inference time for high-resolution  $2048 \times 2048$  images.





Figure 9. **Ablation study.** **Top:** We ablate on the modules of ResAdapter. Baseline represents Dreamshaper, which is a personalized diffusion model based on SD1.5 [30]. The third column represents only ResCLoRA integrated into the model. The fourth column represents only ResENorm integrated into the model. The fifth column represents both them integrated into the model. **Bottom:** We ablate on the alpha of ResAdapter  $\alpha_r$ , from 0 to 1 at lower and higher resolutions.

## References

- [1] Omer Bar-Tal, Lior Yariv, Yaron Lipman, and Tali Dekel. Multidiffusion: Fusing diffusion paths for controlled image generation. 2023. 2, 3, 6, 7
- [2] Shoufa Chen, Chongjian Ge, Zhan Tong, Jiangliu Wang, Yibing Song, Jue Wang, and Ping Luo. Adaptformer: Adapting vision transformers for scalable visual recognition. *Advances in Neural Information Processing Systems*, 35:16664–16678, 2022. 4
- [3] Yukang Chen, Shengju Qian, Haotian Tang, Xin Lai, Zhi-jian Liu, Song Han, and Jiaya Jia. Longlora: Efficient fine-tuning of long-context large language models. *arXiv preprint arXiv:2309.12307*, 2023. 5
- [4] Civitai. Civitai, 2022. 2, 6, 7, 14
- [5] Prafulla Dhariwal and Alexander Nichol. Diffusion models beat gans on image synthesis. *Advances in neural information processing systems*, 34:8780–8794, 2021. 3
- [6] Patrick Esser, Robin Rombach, and Bjorn Ommer. Taming transformers for high-resolution image synthesis. In *Proceedings of the IEEE/CVF conference on computer vision and pattern recognition*, pages 12873–12883, 2021. 3
- [7] Rui Gao and Weiwei Liu. Ddgr: continual learning with deep diffusion-based generative replay. In *International Conference on Machine Learning*, pages 10744–10763. PMLR, 2023. 4, 6
- [8] Ian Goodfellow, Jean Pouget-Abadie, Mehdi Mirza, Bing Xu, David Warde-Farley, Sherjil Ozair, Aaron Courville, and Yoshua Bengio. Generative adversarial networks. *Communications of the ACM*, 63(11):139–144, 2020. 3
- [9] Moayed Haji-Ali, Guha Balakrishnan, and Vicente Ordonez. Elasticdiffusion: Training-free arbitrary size image generation. *arXiv preprint arXiv:2311.18822*, 2023. 2, 3, 6, 7, 10, 14
- [10] Kaiming He, Xiangyu Zhang, Shaoqing Ren, and Jian Sun. Deep residual learning for image recognition. In *Proceedings of the IEEE conference on computer vision and pattern recognition*, pages 770–778, 2016. 4
- [11] Jack Hessel, Ari Holtzman, Maxwell Forbes, Ronan Le Bras, and Yejin Choi. Clipscore: A reference-free evaluation metric for image captioning. *arXiv preprint arXiv:2104.08718*, 2021. 6
- [12] Martin Heusel, Hubert Ramsauer, Thomas Unterthiner, Bernhard Nessler, and Sepp Hochreiter. Gans trained by a two time-scale update rule converge to a local nash equilibrium. *Advances in neural information processing systems*, 30, 2017. 6

- [13] Jonathan Ho, Ajay Jain, and Pieter Abbeel. Denoising diffusion probabilistic models. *Advances in neural information processing systems*, 33:6840–6851, 2020. 2, 3, 4
- [14] Neil Houlsby, Andrei Giurgiu, Stanislaw Jastrzebski, Bruna Morrone, Quentin De Laroussilhe, Andrea Gesmundo, Mona Attariyan, and Sylvain Gelly. Parameter-efficient transfer learning for nlp. In *International Conference on Machine Learning*, pages 2790–2799. PMLR, 2019. 4
- [15] Edward J Hu, Yelong Shen, Phillip Wallis, Zeyuan Allen-Zhu, Yuanzhi Li, Shean Wang, Lu Wang, and Weizhu Chen. Lora: Low-rank adaptation of large language models. *arXiv preprint arXiv:2106.09685*, 2021. 2, 3, 4, 5
- [16] Álvaro Barbero Jiménez. Mixture of diffusers for scene composition and high resolution image generation. *arXiv preprint arXiv:2302.02412*, 2023. 2, 3
- [17] Tero Karras, Miika Aittala, Timo Aila, and Samuli Laine. Elucidating the design space of diffusion-based generative models. *Advances in Neural Information Processing Systems*, 35:26565–26577, 2022. 3
- [18] Diederik P Kingma and Jimmy Ba. Adam: A method for stochastic optimization. *arXiv preprint arXiv:1412.6980*, 2014. 6
- [19] Doyup Lee, Chihyeon Kim, Saehoon Kim, Minsu Cho, and Wook-Shin Han. Autoregressive image generation using residual quantization. In *Proceedings of the IEEE/CVF Conference on Computer Vision and Pattern Recognition*, pages 11523–11532, 2022. 3
- [20] Dongze Lian, Daquan Zhou, Jiashi Feng, and Xinchao Wang. Scaling & shifting your features: A new baseline for efficient model tuning. *Advances in Neural Information Processing Systems*, 35:109–123, 2022. 4
- [21] Cheng Lu, Yuhao Zhou, Fan Bao, Jianfei Chen, Chongxuan Li, and Jun Zhu. Dpm-solver: A fast ode solver for diffusion probabilistic model sampling in around 10 steps. *Advances in Neural Information Processing Systems*, 35:5775–5787, 2022. 14
- [22] Andreas Lugmayr, Martin Danelljan, Andres Romero, Fisher Yu, Radu Timofte, and Luc Van Gool. Repaint: Inpainting using denoising diffusion probabilistic models. In *Proceedings of the IEEE/CVF Conference on Computer Vision and Pattern Recognition*, pages 11461–11471, 2022. 2
- [23] Simian Luo, Yiqin Tan, Suraj Patil, Daniel Gu, Patrick von Platen, Apolinário Passos, Longbo Huang, Jian Li, and Hang Zhao. Lcm-lora: A universal stable-diffusion acceleration module. *arXiv preprint arXiv:2311.05556*, 2023. 3, 9, 10, 14, 20
- [24] Sergi Masip, Pau Rodriguez, Tinne Tuytelaars, and Gido M van de Ven. Continual learning of diffusion models with generative distillation. *arXiv preprint arXiv:2311.14028*, 2023. 4, 6
- [25] Chenlin Meng, Yutong He, Yang Song, Jiaming Song, Jiajun Wu, Jun-Yan Zhu, and Stefano Ermon. Sedit: Guided image synthesis and editing with stochastic differential equations. In *International Conference on Learning Representations*, 2021. 2
- [26] Augustus Odena, Christopher Olah, and Jonathon Shlens. Conditional image synthesis with auxiliary classifier gans. In *International conference on machine learning*, pages 2642–2651. PMLR, 2017. 3
- [27] Dustin Podell, Zion English, Kyle Lacey, Andreas Blattmann, Tim Dockhorn, Jonas Müller, Joe Penna, and Robin Rombach. Sdxl: Improving latent diffusion models for high-resolution image synthesis. *arXiv preprint arXiv:2307.01952*, 2023. 2, 3, 4, 5, 6, 7, 8, 14
- [28] Alec Radford, Luke Metz, and Soumith Chintala. Unsupervised representation learning with deep convolutional generative adversarial networks. 2015. 3
- [29] Aditya Ramesh, Prafulla Dhariwal, Alex Nichol, Casey Chu, and Mark Chen. Hierarchical text-conditional image generation with clip latents. *arXiv preprint arXiv:2204.06125*, 1(2):3, 2022. 2
- [30] Robin Rombach, Andreas Blattmann, Dominik Lorenz, Patrick Esser, and Björn Ommer. High-resolution image synthesis with latent diffusion models. In *Proceedings of the IEEE/CVF conference on computer vision and pattern recognition*, pages 10684–10695, 2022. 2, 3, 4, 5, 6, 7, 9, 11, 14
- [31] Olaf Ronneberger, Philipp Fischer, and Thomas Brox. U-net: Convolutional networks for biomedical image segmentation. In *Medical Image Computing and Computer-Assisted Intervention—MICCAI 2015: 18th International Conference, Munich, Germany, October 5-9, 2015, Proceedings, Part III 18*, pages 234–241. Springer, 2015. 2
- [32] Nataniel Ruiz, Yuanzhen Li, Varun Jampani, Yael Pritch, Michael Rubinstein, and Kfir Aberman. Dreambooth: Fine tuning text-to-image diffusion models for subject-driven generation. In *Proceedings of the IEEE/CVF Conference on Computer Vision and Pattern Recognition*, pages 22500–22510, 2023. 2, 3
- [33] Christoph Schuhmann, Romain Beaumont, Richard Vencu, Cade Gordon, Ross Wightman, Mehdi Cherti, Theo Coombes, Aarush Katta, Clayton Mullis, Mitchell Wortsman, et al. Laion-5b: An open large-scale dataset for training next generation image-text models. *Advances in Neural Information Processing Systems*, 35:25278–25294, 2022. 2, 3, 4, 5, 6, 21
- [34] Christoph Schuhmann, Richard Vencu, Romain Beaumont, Robert Kaczmarczyk, Clayton Mullis, Aarush Katta, Theo Coombes, Jenia Jitsev, and Aran Komatsuzaki. Laion-400m: Open dataset of clip-filtered 400 million image-text pairs. *arXiv preprint arXiv:2111.02114*, 2021. 5, 7
- [35] James Seale Smith, Yen-Chang Hsu, Lingyu Zhang, Ting Hua, Zsolt Kira, Yilin Shen, and Hongxia Jin. Continual diffusion: Continual customization of text-to-image diffusion with c-lora. *arXiv preprint arXiv:2304.06027*, 2023. 4, 6
- [36] Jiaming Song, Chenlin Meng, and Stefano Ermon. Denoising diffusion implicit models. In *International Conference on Learning Representations*, 2020. 2
- [37] Jiaming Song, Chenlin Meng, and Stefano Ermon. Denoising diffusion implicit models. *arXiv preprint arXiv:2010.02502*, 2020. 14
- [38] Yang Song, Jascha Sohl-Dickstein, Diederik P Kingma, Abhishek Kumar, Stefano Ermon, and Ben Poole. Score-based generative modeling through stochastic differential equations. *arXiv preprint arXiv:2011.13456*, 2020. 2, 3

- [39] Aaron Van Den Oord, Oriol Vinyals, et al. Neural discrete representation learning. *Advances in neural information processing systems*, 30, 2017. 3, 4
- [40] Ashish Vaswani, Noam Shazeer, Niki Parmar, Jakob Uszkoreit, Llion Jones, Aidan N Gomez, Łukasz Kaiser, and Illia Polosukhin. Attention is all you need. *Advances in neural information processing systems*, 30, 2017. 4
- [41] Enze Xie, Lewei Yao, Han Shi, Zhili Liu, Daquan Zhou, Zhaoqiang Liu, Jiawei Li, and Zhenguo Li. Diffit: Unlocking transferability of large diffusion models via simple parameter-efficient fine-tuning. *arXiv preprint arXiv:2304.06648*, 2023. 2, 4
- [42] Runxin Xu, Fuli Luo, Zhiyuan Zhang, Chuanqi Tan, Baobao Chang, Songfang Huang, and Fei Huang. Raise a child in large language model: Towards effective and generalizable fine-tuning. *arXiv preprint arXiv:2109.05687*, 2021. 4
- [43] Hu Ye, Jun Zhang, Sibio Liu, Xiao Han, and Wei Yang. Ip-adapter: Text compatible image prompt adapter for text-to-image diffusion models. *arXiv preprint arXiv:2308.06721*, 2023. 3, 9, 10, 14, 19
- [44] Lvmin Zhang, Anyi Rao, and Maneesh Agrawala. Adding conditional control to text-to-image diffusion models. In *Proceedings of the IEEE/CVF International Conference on Computer Vision*, pages 3836–3847, 2023. 3, 9, 10, 14, 18
- [45] Wenliang Zhao, Lujia Bai, Yongming Rao, Jie Zhou, and Jiwen Lu. Unipc: A unified predictor-corrector framework for fast sampling of diffusion models. *Advances in Neural Information Processing Systems*, 36, 2024. 14
- [46] Qingping Zheng, Yuanfan Guo, Jiankang Deng, Jianhua Han, Ying Li, Songcen Xu, and Hang Xu. Any-size-diffusion: Toward efficient text-driven synthesis for any-size hd images. *arXiv preprint arXiv:2308.16582*, 2023. 2, 3



## Appendix

### 7. Detailed Inference Setup

We set up detailed inference settings about ResAdapter integrated into the base model (e.g., SD [30] and SDXL [27]), the personalized models [4], ControlNet [44], IP-Adapter [43], LCM-LoRA [23], and ElasticDiffusion (ED) [9].

1. For the base model, we select the corresponding prompt generation images from SD and SDXL. We reference SD to generate images in 50 steps with CFG=7.5 and choose DDIM [37] as the scheduler.
2. For the personalized model, we select the corresponding prompt from CivitAI [4] to generate imaginative images to stimulate the creativity of the personalized model. We generate images in 25 steps with CFG=10 and choose DPM Solver [21] as the scheduler.
3. For ControlNet, we select the appropriate images and prompts from [44]. For the canny condition, for example, we extract the canny condition from the input image, where the thresholds are set to 100 and 200. We generate the images in 25 steps with CFG=7.5 and choose UniPC [45] as the scheduler.
4. For IP-Adapter, we select the input image and prompt from [43]. we complete the image variation and inpainting tasks. We generate the images in 50 steps with CFG=7.5 and choose DDIM as the scheduler.
5. For LCM-LoRA, we generate images based on the personalized model. We generate images in 4 steps with CFG=1, and choose LCM scheduler [23].
6. For ElasticDiffusion, we generate images with the personalized model. For example, Dreamshaper-XL generates a 2048x2048 image and we generate a 1024x1024 image for post-processing. After inserting the ResAdapter, we generated a  $768 \times 768$  image for post-processing. We follow the default post-processing parameters of the ED [9], we generated the image in 25 steps with CFG=7.5, and we choose DDIM as the scheduler.

### 8. Additional Qualitative Results

**ResAdapter with Personalized Models.** We present additional qualitative results of the personalized diffusion model in Fig.10-12. Each comparison set consists of two images: the left image shows the personalized model with the ResAdapter, and the right image shows the personalized model without the ResAdapter. ResAdapter significantly enhances the quality of images with unrestricted resolutions and aspect ratio without transforming their original style domain.

**ResAdapter with Other Modules.** We provide more qualitative results for ControlNet in Fig.13, IP-Adapter in Fig.14 and LCM-LoRA in Fig.15. ResAdapter can enhance the quality of resolution-free generation images with other modules.

### 9. Ablation Study for Trained Modules

The ablation study for the trainable modules of ResAdapter is shown in Fig. 16. We visualize the three groups of LoRA insertions on the personalized diffusion models. ResAdapter maintains style domain consistency (Realism style), while both the ResNet LoRA and the vanilla LoRA influence its original style domain. Meanwhile, we visualize the two sets of normalization loaded on the personalized diffusion model (Cute style). ResAdapter does not compromise the image domain, while all normalization layers severely degrade the image quality.

### 10. Limitation and Future Work

In our experiments, we find that most failure cases occur when the general prompts are input into the personalized diffusion models. It leads that the image generation capability in personalized models is not activated correctly. In this case, the role of ResAdapter in resolution interpolation and extrapolation is difficult to highlight. A potential solution is to correct the user prompts with a large language model, which we leave for future work. Additionally, we consider to use super-resolution models to speed up generation of higher-resolution images.

*Text-to-image, Dreamshaper-XL (SDXL)*



Figure 10. **Qualitative results** about the text-to-image generation task. The baseline represents DreamshaperXL. For each pair of images, the left side is from ResAdapter with baseline and the right side is from baseline.



*Text-to-image, Dreamlike (SD1.5)*



Figure 11. **Qualitative results** about the text-to-image generation task. The baseline represents Dreamlike. For each pair of images, the left side is from ResAdapter with baseline and the right side is from baseline.





Figure 12. **Qualitative results** about the text-to-image generation task. The baseline represents Dreamshaper or AnimeArtXL. For each pair of images, the left side is from ResAdapter with baseline and the right side is from baseline.



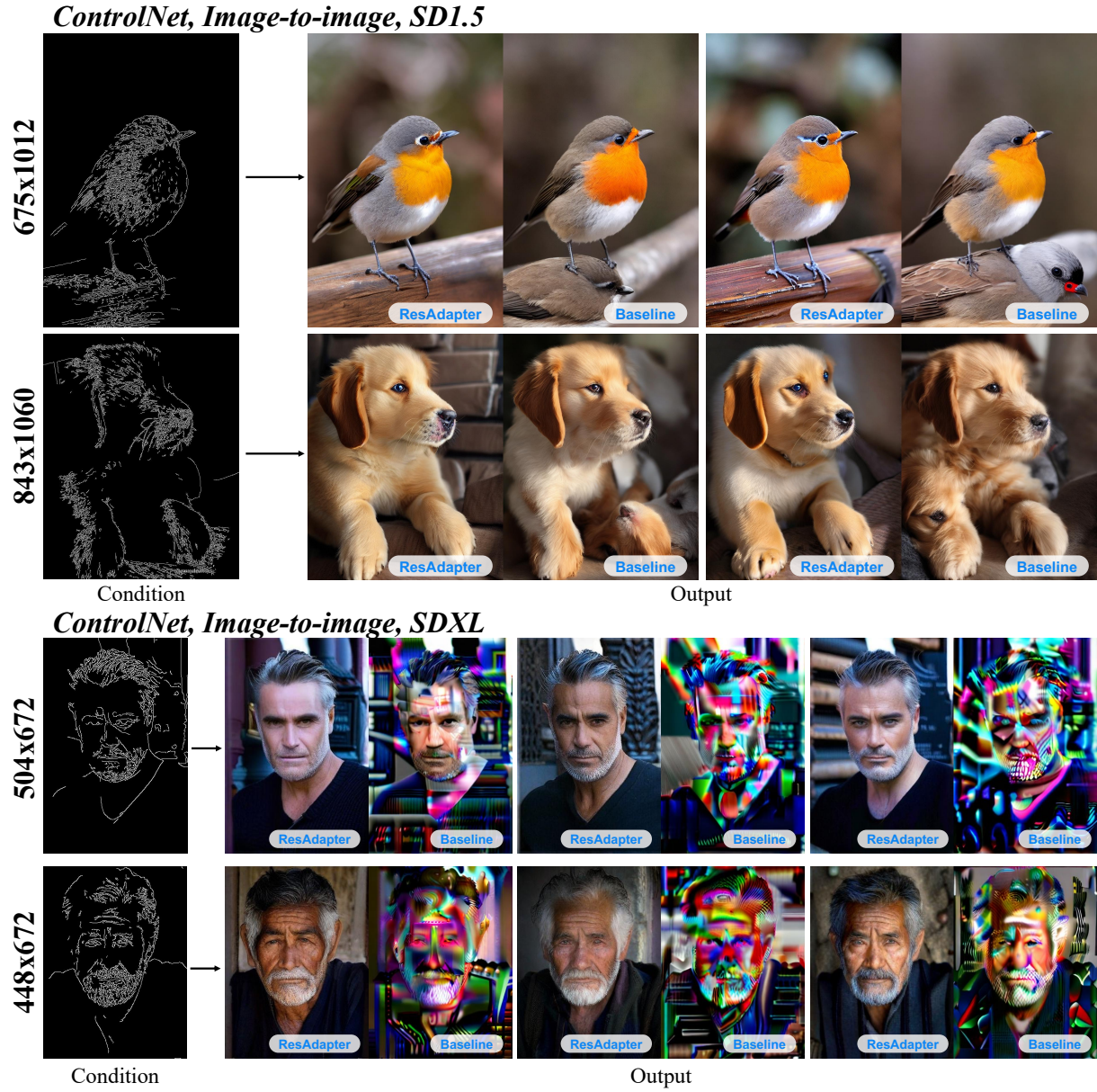


Figure 13. **Qualitative results** about the image-to-image generation task. The baseline represents ControlNet [44]. For each pair of images, the left side is from ResAdapter with baseline and the right side is from baseline.



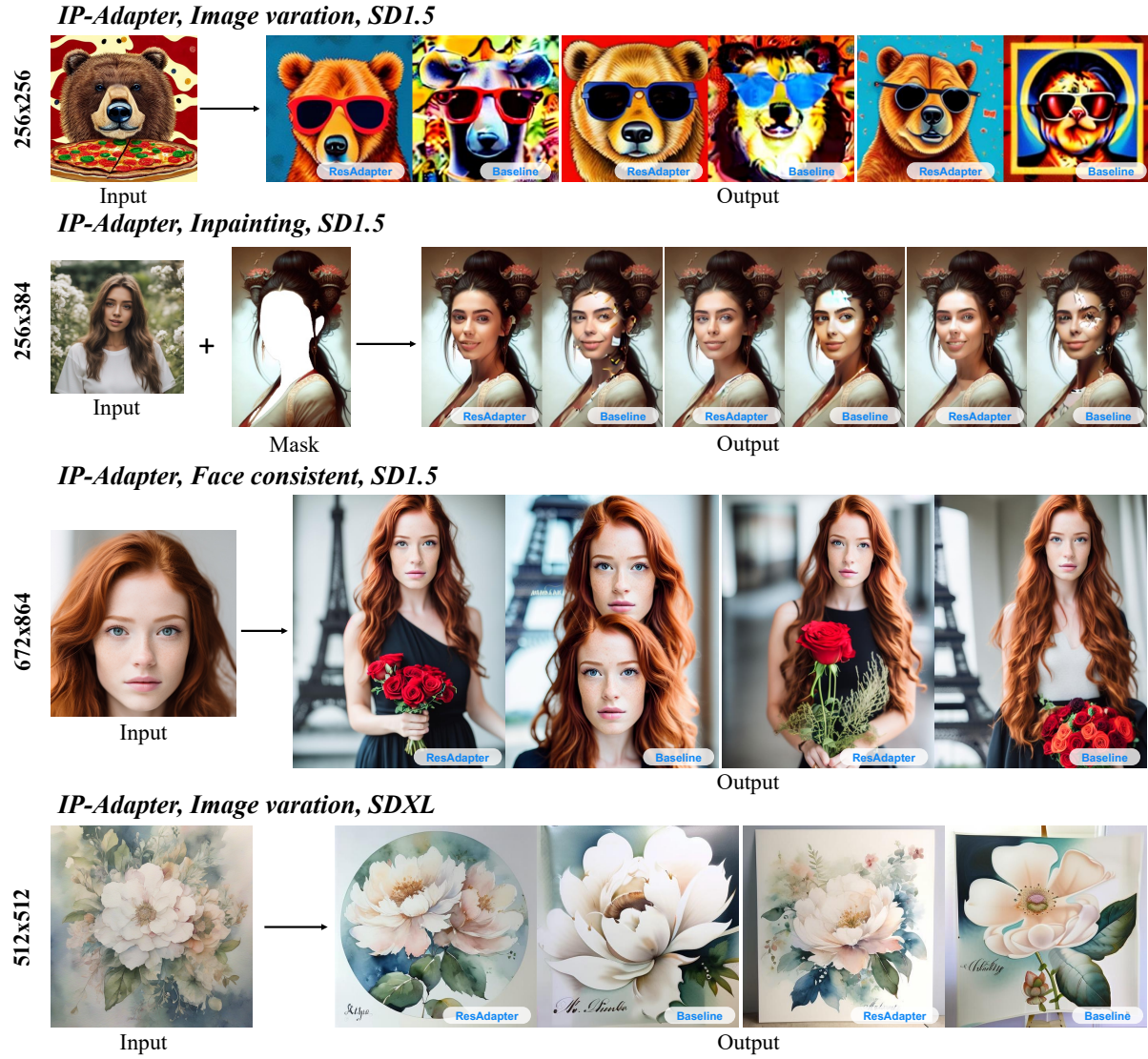
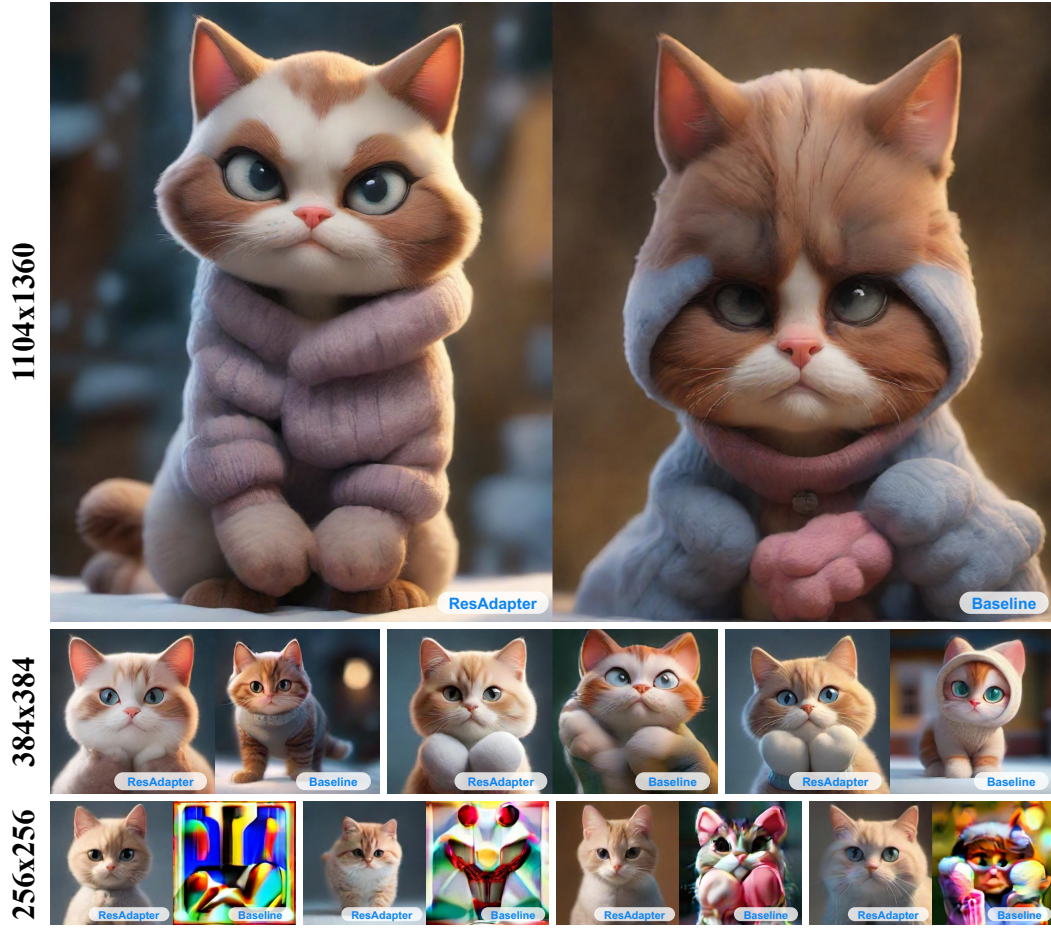


Figure 14. **Qualitative results.** The baseline represents IP-Adapter [43]. For each pair of images, the left side is from ResAdapter with baseline and the right side is from baseline.

*LCM-LoRA, Text-to-image, Samaritan3dCartoon (SDXL)*



*LCM-LoRA, Text-to-image, Dreamshaper-XL (SDXL)*

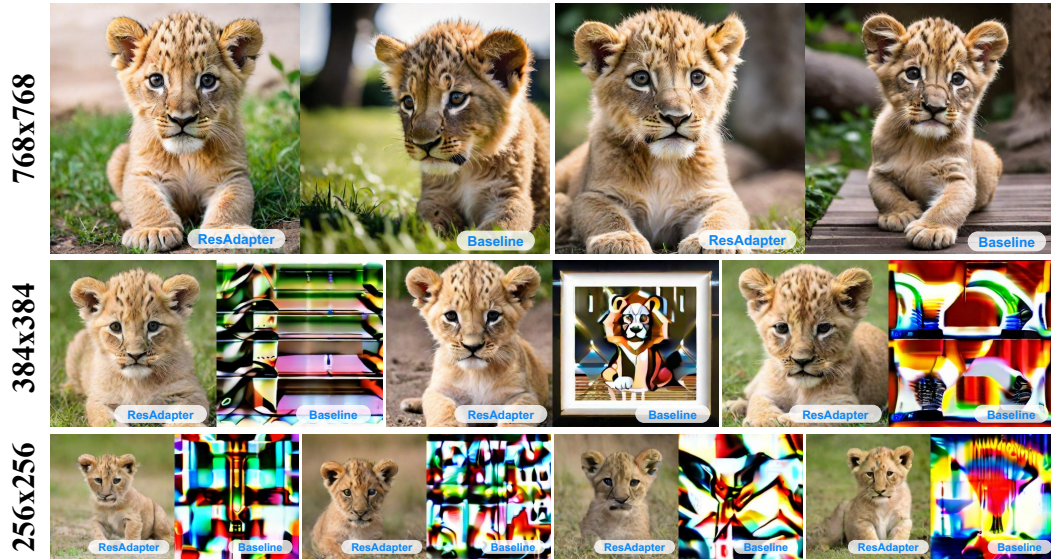


Figure 15. **Qualitative results** about the accelerating text-to-image task. The baseline represents Samaritan3dXL with LCM-LoRA [23] or DreamshaperXL with LCM-LoRA. For each pair of images, the left side is from ResAdapter with baseline and the right side is from baseline.



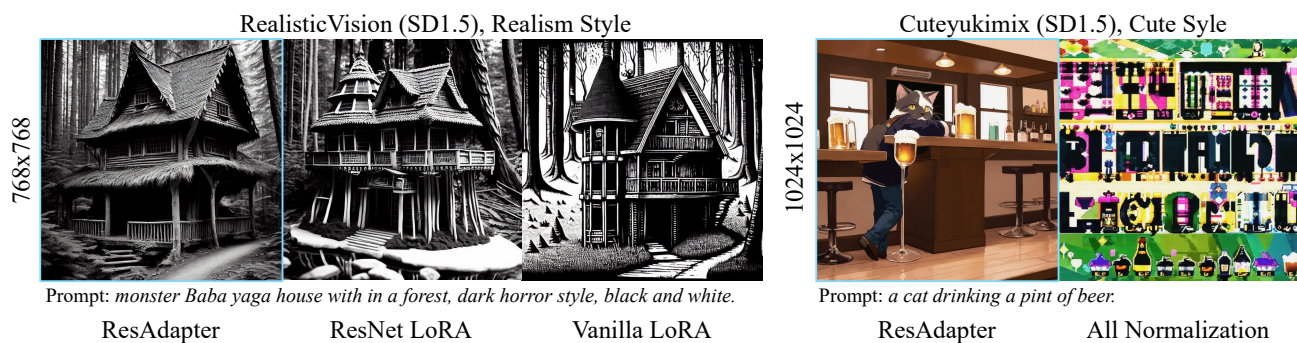


Figure 16. **Left:** ResNet-LoRA represents LoRA weights on the resnet block. All-LoRA represents LoRA weights on the resnet layer and the attention layer. **Right:** All-Normalization represents the layer normalization of attention layer and the group normalization of resnet layer. We train them on LAION-5B [33].